

STUDY OF NON-TRIVIAL BEHAVIOR IN THE ANALYSIS OF $^{58}\text{Ni} + ^{27}\text{Al}$ ELASTIC SCATTERING AROUND THE COULOMB BARRIER

KAMALA KANTA JENA^{a,b}, SANTOSH KUMAR AGARWALLA^b
BIDHUBHUSAN SAHU^{c,†}

^aP.G. Department of Physics, Bhadrak Autonomous College
Bhadrak-756100, India

^bDepartment of Applied Physics and Ballistics
Fakir Mohan University, Balasore-756019, India

^cSchool of Applied Sciences, KIIT Deemed to be University
Bhubaneswar-751024, India

*Received 28 June 2022, accepted 5 September 2022,
published online 19 October 2022*

A new form of potential is used to treat the optical model unequivocally for the analysis of scattering results of the $^{58}\text{Ni} + ^{27}\text{Al}$ system. The phenomenological optical potential is formed with the Ginocchio potential for analysis near the Coulomb barrier. Theoretical calculations explain the experimental outcomes over a wide range of colliding energies, and hence exhibit *threshold anomaly*. An inbuilt non-trivial behaviour in the formulation near the Coulomb barrier position is found essential for a successful explanation of the experimental results.

DOI:10.5506/APhysPolB.53.10-A1

1. Introduction

Interaction between two nucleons is the basic interaction in nuclear physics. This can be a phenomenological representation with proper radial dependence with the help of nuclear scattering experiments. In principle, the knowledge of such interaction can explore all properties of nuclei, but the case is not so in practice. Rather the properties are studied by taking the help of proper scattering experiments and reaction measurements [1, 2].

Not all the experiments involve the interaction of only nucleons with nuclei. The interaction may involve alpha particles, deuterons, and many other particles of composite nature. Superposition of contributing interactions is considered in such situations. Various properties of nuclei can be

[†] Corresponding author: bbsahufpy@kiit.ac.in

determined by nucleus–nucleus scattering experiments at low- and medium-energy ranges. The results so obtained can be analyzed by different models of macroscopic and microscopic nature; the optical model is one of those models. The versatility of an optical model is evident from the applicability of the model even in the case of many complicated nuclear phenomena for analysis. We may cite the examples of Woods–Saxon potential, Gaussian potential, modified Woods–Saxon potentials, and some others which are used in optical model analysis.

The real and imaginary parts of the optical potential show interesting variations around the Coulomb barrier in the elastic scattering [3–7] of heavy ions ($A \geq 4$). In the case of tightly bound heavy projectiles, the real part of the potential shows a quick rise when the magnitude of colliding energy becomes very close to the Coulomb barrier. It attains its maximum at the barrier and then shows a slow fall as the incident energy decreases below the Coulomb potential. Interestingly, the real part hardly shows prominent variation at higher magnitudes of colliding energies. Thus, the course of variation follows a near bell-shaped curve around the Coulomb barrier.

The variation in the case of the imaginary part is different in the same vicinity. It remains nearly constant at higher energy but decreases to a low value around the barrier [7–13]. The phenomenon is referred to as *threshold anomaly* (TA). TA phenomena take place due to the coupling of different reaction channels; the channels being both elastic and quasi-elastic. The anomaly in variations observed in the real and imaginary parts with colliding energy of the projectile can be explained by dispersion relation, which is realized from the principle of causality. The dispersion relation of Byron and Fuller [14] may be considered for an explanation of the phenomena. We explain the TA phenomenon by using a potential with few parameters and a significantly small imaginary part.

We consider a heavy-ion elastic collision system $^{58}\text{Ni} + ^{27}\text{Al}$, which is semi-classical due to the big mass and large size of the particles involved. The experimental data of the system are explained within the framework of an optical model by using complex potential with suitable parameters. Experimental measurement and theoretical analysis of scattering angular distribution data of the elastic system are obtained from Brandan *et al.* [15]. The angular distributions are measured with nickel beams (^{58}Ni) at five energies from 48.8 to 69.5 MeV in the centre-of-mass (c.m.) frame. We consider this system to extend the variation in the study of elastic scattering with special attention to TA. A large change in the real part near the Coulomb barrier was found for the system $^{16}\text{O} + ^{208}\text{Pb}$ [7, 9], but the variation was small in the cases of $^{32}\text{S} + ^{32}\text{S}$ [16], $^{32}\text{S} + ^{40}\text{Ca}$ [13], and $^{35}\text{Cl} + ^{24}\text{Mg}$ [17]. The scattering data were measured by Sugiyama *et al.* [18, 19] for the systems $^{28}\text{Si} + ^{58}\text{Ni}$, $^{28}\text{Si} + ^{62}\text{Ni}$, and $^{28}\text{Si} + ^{64}\text{Ni}$, while Brandan *et al.*

[15] considered a neighbouring system $^{58}\text{Ni} + ^{27}\text{Al}$. We are interested in the system $^{58}\text{Ni} + ^{27}\text{Al}$ to explain the experimental results by our optical potential for the same energy range. Consideration of the system with an aluminium target helps us realize the versatility of our potential in analyzing light targets in addition to comparably heavier targets such as ^{90}Zr [20] and ^{56}Fe [21].

We use a phenomenological optical potential [22, 23] based on a short-ranged, smooth, and analytically solvable asymmetric potential developed by Ginocchio [24]. Our potential has significantly fewer parameters. The potential consists of two analytically solvable regions, namely, the inner (volume) region and the outer (surface) region. The regions are smoothly joined near $r = R_0$. We refer the location to an analytic junction, because the junction is analytically solvable and the Schrödinger equation can be solved there. Mallick *et al.* in [22] have explained the results of $^{16}\text{O} + ^{28}\text{Si}$ scattering experiment over a large range of energy by using this potential. The inbuilt non-trivial behaviour near the Coulomb barrier position is an important feature of the potential used. The feature helps us explain the experimental data of the collision system with a tightly bound nickel (^{58}Ni) projectile. We also find the phenomena of ‘threshold anomaly’ in systems $^{14}\text{N} + ^{90}\text{Zr}$ [20] and $^{14}\text{N} + ^{56}\text{Fe}$ [21] with the fast rise of the absorptive imaginary part, accompanied by a rapid fall of the real part of potential when the incident energy magnitude rises above their respective Coulomb barriers.

The optical potentials used in some papers bear large imaginary parts, in which substantial absorption of partial waves may take place. On the contrary, Brandan *et al.* [15] fix the volume imaginary term at a low value in comparison to the high real part but vary the surface component to fit the data. The ratio between imaginary-to-real parts remains at 0.04 for the entire range of incident energy. The small ratio is less effective in destroying resonance states if at all generated by volume part in effective potential.

We organized our illustration to discuss the formulation of the optical potential in Section 2. The sub-sections contained in Section 3 explain the application of the formulation for elastic scatterings of the tightly bound heavy projectile on the aluminium target at energies close to the Coulomb barrier and describe the TA phenomenon. The dependence of reflection function $|S_l|$ upon ‘ l ’ is studied for each contributing partial wave. Finally, Section 4 presents the summary of the analysis and main conclusions of the task.

2. Formulation of theory

Nuclear interactions are described by a potential comprising the Coulomb potential $V_C(r)$, the nuclear potential $V_N(r)$, and a centrifugal part V_{CF} . Their combined effect or effective potential $V_{\text{eff}}(r)$ for the reduced system of

nuclear collision with reduced mass μ can be given by

$$V_{\text{eff}} = V_{\text{C}}(r) + V_{\text{N}}(r) + V_{\text{CF}}. \quad (1)$$

The term

$$V_{\text{CF}} \sim \frac{l(l+1)\hbar^2}{2\mu r^2}$$

describes the potential as a contribution from the centrifugal force. The nuclear potential is given in complex form, *i.e.*, $V_{\text{N}}(r) = V_n(r) + iW_n(r)$. The real part [23] of the nuclear potential is represented by

$$V_n(r) = \begin{cases} \frac{-V_B}{B_1} [B_0 + (B_1 - B_0)(1 - y_1^2)] & \text{if } 0 < r < R_0, \\ \frac{-V_B}{B_2} [B_2(1 - y_2^2)] & \text{if } r \geq R_0. \end{cases} \quad (2)$$

With substitutions of $y = \tanh \rho_n$, $\rho_n = (r - R_0)b_n$, and $V_B = V_{01}B_1 = V_{02}B_2$, the real part becomes

$$V_n(r) = \begin{cases} -V_{01} \left[B_0 + \frac{(B_1 - B_0)}{\cosh^2 \rho_1} \right] & \text{if } 0 < r < R_0, \\ -V_{02} \left[\frac{B_2}{\cosh^2 \rho_2} \right] & \text{if } r \geq R_0. \end{cases} \quad (3)$$

The parameter b_n is known as the slope parameter and is given by $b_n = \frac{\sqrt{2mV_B}}{\hbar^2 B_n}$ for which $n = 1, 2$. In Eq. (3), R_0 represents the radial distance in the surface region which is close to the radial position of the effective S -wave barrier potential. The potential depth at origin $r = 0$ is controlled by B_0 , whereas parameter V_B gives a measure of potential depth at $r = R_0$. Parameter B_n controls b_n on both sides of R_0 , and so does the other parameter V_B . A little change in B_n results in a large variation in the potential, and b_n changes largely. Figure 1 describes the real part $V_n(r)$ of nuclear potential with the parameters mentioned. The potential we use possesses an interesting feature that is different from the usual potential behaviour. Unlike monotonous fall of potential with distance ' r ' in the case of standard Woods-Saxon potential, our potential shows neck-formation near $r = R_0$, where two sections of the potential corresponding to the volume region (slope b_1) and the surface region (slope b_2) meet to satisfy analytic continuity. The feature ensures indifference in two parts of the potential and keeps their derivatives the same at that position as well. Such a potential takes care of phenomena such as the effects of frictional forces and resonance in the formation of a composite binuclear system. It can transfer nucleon(s) of the target to the projectile and of a projectile to the target in the surface region as the bombarding nuclei interact with each other. This non-trivial

feature helps fit cross sections suitably at various energies for the system considered. This is further explained in Fig. 7 in Section 4. The non-trivial behaviour does not impose any irregularity in amplitude variation of the wave function with the varying radial distance.

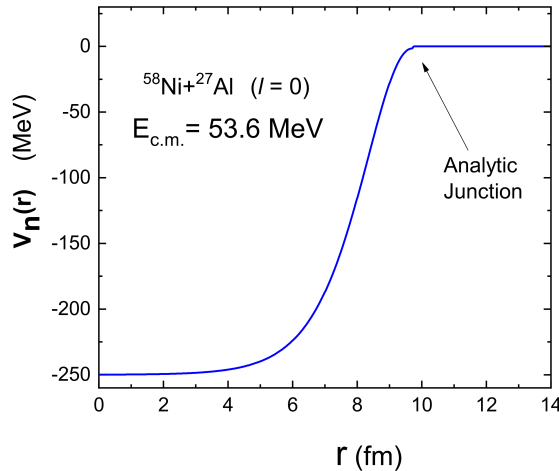


Fig. 1. The real part $V_n(r)$ of the nuclear potential for the scattering system $^{58}\text{Ni} + ^{27}\text{Al}$ plotted against the radial distance ' r ' at incident energy $E_{\text{cm}} = 53.6$ MeV. Parameters taken are $R_0 = 9.7$ fm, $B_0 = 250$ MeV, $B_1 = 6.0$, $B_2 = 1.0$ and $V_B = 1.6$ MeV. The arrow indicates the position of analytic junction.

The imaginary part $W_n(r)$ of the potential can be represented in a similar fashion as that of the real part. Of course, their strengths differ. By substituting $V_{0nW} = V_{BW}/W_n$, the imaginary part is given by Eq. (4) and its behaviour is depicted in Fig. 2 with suitable parameterization

$$W_n(r) = \begin{cases} -V_{01W} \left[W_0 + \frac{(W_1 - W_0)}{\cosh^2 \rho_1} \right] & \text{if } 0 < r < R_{0W}, \\ -V_{02W} \left[\frac{W_2}{\cosh^2 \rho_2} \right] & \text{if } r \geq R_{0W}. \end{cases} \quad (4)$$

The Coulomb potential for the scattering system is given by

$$V_C(r) = \begin{cases} \frac{Z_P Z_T e^2}{2R_C^3} (3R_C^2 - r^2) & \text{if } r < R_C, \\ \frac{Z_P Z_T e^2}{r} & \text{if } r > R_C, \end{cases} \quad (5)$$

where $R_C = r_C(A_P^{1/3} + A_T^{1/3})$; A_P is the mass number of the projectile and A_T is the mass number of the target nucleus. Also, Z_P is the atomic number

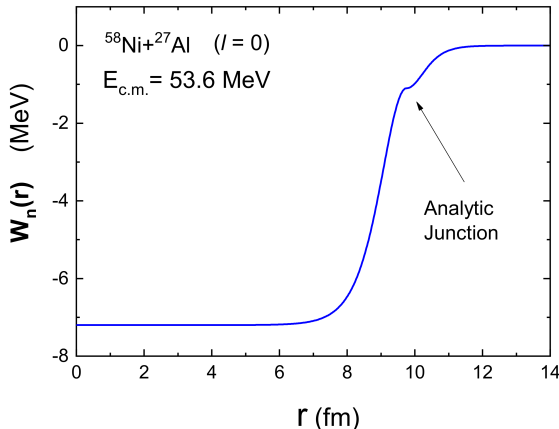


Fig. 2. Presentation of the imaginary part $W_n(r)$ of the nuclear potential against the radial distance (r) for $^{58}\text{Ni} + ^{27}\text{Al}$ system at the incident energy $E_{\text{cm}} = 53.6$ MeV. Parameters are $R_{0W} = 9.75$ fm, $W_0 = 7.2$ MeV, $V_{BW} = 1.1$ MeV, $W_1 = 1.0$ and $W_2 = 1.2$. An arrow indicates the position of analytic junction.

of the projectile and Z_T is the atomic number of the target nucleus. With $l = 0$, Eq. (5) describes the effective potential as

$$V_{\text{eff}}(r) = V_N(r) + V_C(r). \quad (6)$$

The real part (taking $l = 0$) of the effective optical potential is given in Fig. 3 with the parameters which are used for the real part in Fig. 1 and the imaginary part in Fig. 2. The scattering amplitude can be determined by solving Schrodinger's equation. We solve the following Schrodinger equation with the given effective potential $V_{\text{eff}}(r)$ for various partial waves (l) to obtain the total scattering amplitude $f(\theta)$.

$$\left[\frac{-\hbar^2}{2\mu} \nabla^2 + V_{\text{eff}}(r) \right] \psi(\vec{r}) = E\psi(\vec{r}). \quad (7)$$

The total scattering amplitude $f(\theta)$ is expressed as the sum of Coulomb and nuclear scattering amplitudes. $f_C(\theta)$ and $f_N(\theta)$ are the Coulomb scattering amplitude and nuclear scattering amplitude, respectively, then the total scattering amplitude is given by

$$f(\theta) = f_C(\theta) + f_N(\theta). \quad (8)$$

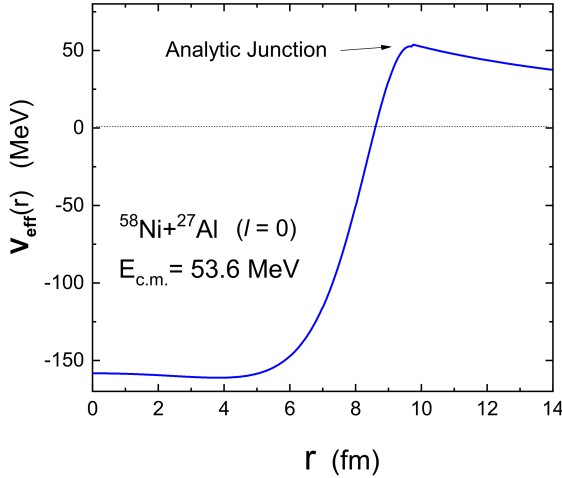


Fig. 3. The effective optical potential $V_{\text{eff}}(r)$ for $l = 0$ for $^{58}\text{Ni} + ^{27}\text{Al}$ at $E_{\text{cm}} = 53.6$ MeV against the radial distance (r). Parameters are $R_0 = 9.7$ fm, $B_0 = 250$ MeV, $B_1 = 6.0$, $B_2 = 1.0$, $V_B = 1.6$ MeV, $R_{0W} = 9.75$ fm, $W_0 = 7.2$ MeV, $V_{BW} = 1.1$ MeV, $W_1 = 1.0$ and $W_2 = 1.2$. The arrow indicates the position of analytic junction in the effective potential.

The nuclear amplitude $f_N(\theta)$ and the Coulomb amplitude $f_C(\theta)$ have expansions as follows:

$$f_N(\theta) = \frac{1}{2ik} \sum_l (2l+1) e^{2i\sigma_l} \left(e^{2i\delta_l} - 1 \right) P_l(\cos \theta), \quad (9)$$

$$f_C(\theta) = \frac{1}{2ik} \sum_l (2l+1) \left(e^{2i\delta_l} - 1 \right). \quad (10)$$

The parameter σ_l describes the Coulomb phase shift due to scattering and δ_l describes the nuclear phase shift. The ratio of differential cross section and Coulomb scattering cross section represents the elastic scattering cross section. The differential cross section of the elastic scattering with respect to the Rutherford scattering cross section (σ_{Ruth}) is given by

$$\frac{d\sigma}{d\sigma_{\text{Ruth}}} = \left| \frac{f(\theta)}{f_C(\theta)} \right|^2. \quad (11)$$

Equations (12) and (13) mentioned below describe the partial waves for the elastic scattering cross section σ_{el} and the partial wave reaction cross section

σ_{rl} . The S-matrix for the l^{th} partial wave is represented by S_l

$$\sigma_{el} = \frac{\pi}{k^2}(2l+1)|1 - S_l|^2, \quad (12)$$

$$\sigma_{rl} = \frac{\pi}{k^2}(2l+1)(1 - |S_l|^2). \quad (13)$$

With the above theoretical formalism and potential, the results of the elastic scattering system have been discussed in the following section.

3. Results

While analyzing elastic scattering data for the system $^{58}\text{Ni} + ^{27}\text{Al}$, the potential in the optical model taken by Brandan *et al.* [15] contains a real part and an imaginary part. The imaginary part comprises the volume term and complicated surface term, in which the minimum value (1.5 MeV) differs by 96% from the maximum value (37.67 MeV). The success story of the optical potential generated by the flexible Ginocchio potential [22–24] catalyzes us to explain elastic scattering data and threshold anomaly of the system. The formalism of Section 2 is applied to analyze the experimental data. Theoretical calculations are carried out to measure angular cross sections at different incident energies, and the variations in real and imaginary parts near the Coulomb barrier are studied carefully.

3.1. Study of elastic scattering cross sections

The incident energies in the laboratory frame for the elastic scattering of ^{58}Ni -beam by ^{27}Al -target are taken at 155, 160, 170, 185, and 220 MeV, which are equivalent to 48.8, 50.4, 53.6, 58.3, and 69.5 MeV, respectively, in the c.m.-frame. The Coulomb barrier of the system is present near 50 MeV. The optical model parameters for the best fit are stated in Table 1.

Table 1. Energy-dependent parameters.

E_{cm} [MeV]	V_B [MeV]	W_2 [MeV]	V_{BW} [MeV]
48.8	1.6	1.40	0.4
50.4	1.9	1.20	0.6
53.6	1.6	1.20	1.1
58.3	1.3	1.20	1.24
69.5	1.25	3.90	1.24

Theoretical angular cross sections are compared with experimental values as shown in Fig. 4 for the above incident energies. Experimental data obtained from <http://nrw.jinr.ru> are digitized with GSYS-2.4. Seven parameters of the potential out of ten parameters remain energy-independent.

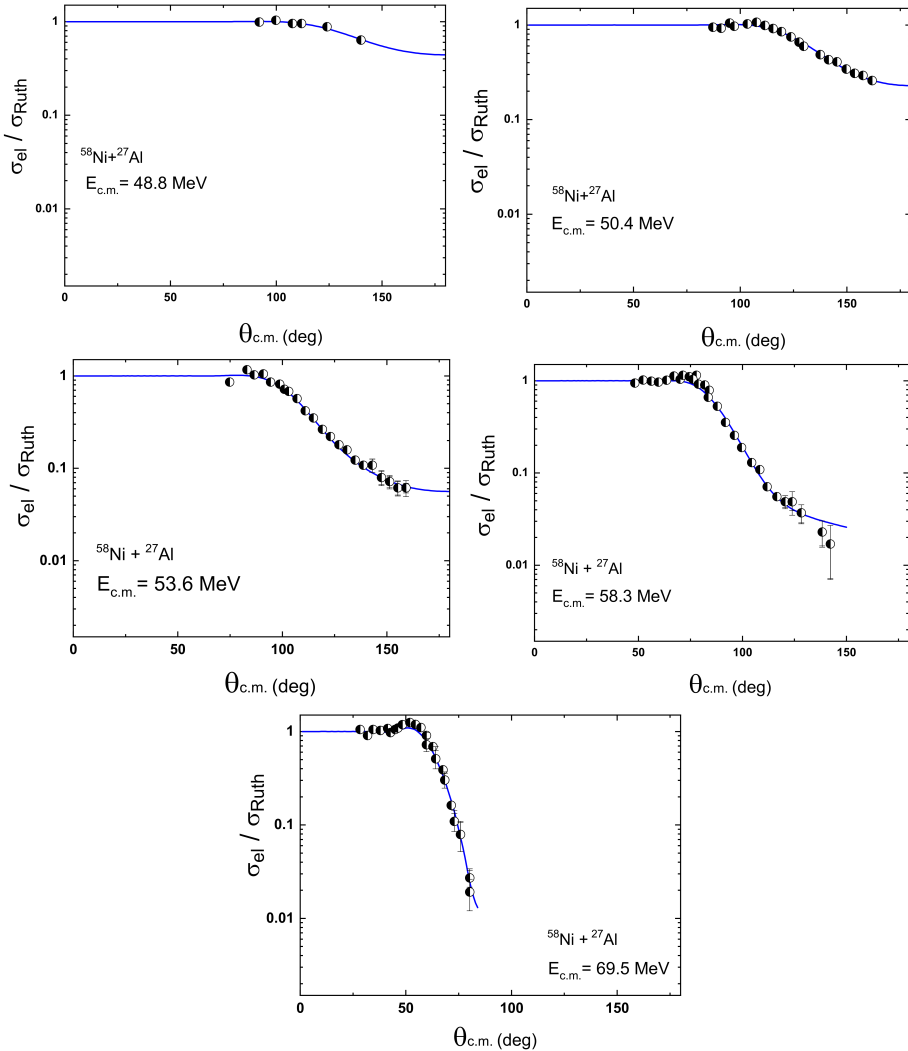


Fig. 4. Plotting of calculated angular cross sections against experimental values at given incident energies for $^{58}\text{Ni} + ^{27}\text{Al}$ with parameters $R_0 = 9.7$ fm, $R_{0W} = 9.75$ fm, $B_0 = 250$ MeV, $B_1 = 6.0$, $B_2 = 1.0$, $W_0 = 7.2$ MeV and $W_1 = 1.0$. In all the figures, half-dark circles represent experimental data and solid-line curves represent theoretical calculations. Experimental data are obtained from Ref. [15].

The radial distance in the surface region R_0 is kept constant at 9.7 fm with energy here. Other independent parameters are found to be $R_{0W} = 9.75$ fm, $B_0 = 250$ MeV, $B_1 = 6.0$, $B_2 = 1.0$, $W_0 = 7.2$ MeV, and $W_1 = 1.0$ for the best fit of theoretical data to experimental results for the entire range of incident energies. Only three parameters V_B , W_2 , and V_{BW} enlisted in Table 1 vary with incident energies. For our entire calculations, we take the Coulomb radius parameter r_C to be 1.25 fm. Theoretical calculations are in fairly good agreement with the experimental results, which is evident from the plots illustrated in Fig. 4. Theoretical calculations in the graphs are represented by solid-line curves, whereas the experimental data [15] are represented by half-dark circles.

No doubt, the optical potential we use takes care of the volume region as well as the surface region. Further, imaginary potentials used in the potential for the best fit are significantly small in comparison to the corresponding real potentials. The real parts of the potential are taken the same, *i.e.*, 250 MeV for all the five incident energies. The imaginary parts are also kept small and the same, *i.e.*, 7.2 MeV in comparison to their counterpart real potentials. Thus, the ratios of imaginary parts to real parts remain the same, *i.e.*, 0.028 for all colliding energies.

3.2. Phenomenon of threshold anomaly

While plotting theoretical data against experimental results, the real and the imaginary parts of the optical potential show the phenomenal variation. Variations found for the best-fit curves at colliding energies near the Coulomb barrier are described in Fig. 5.

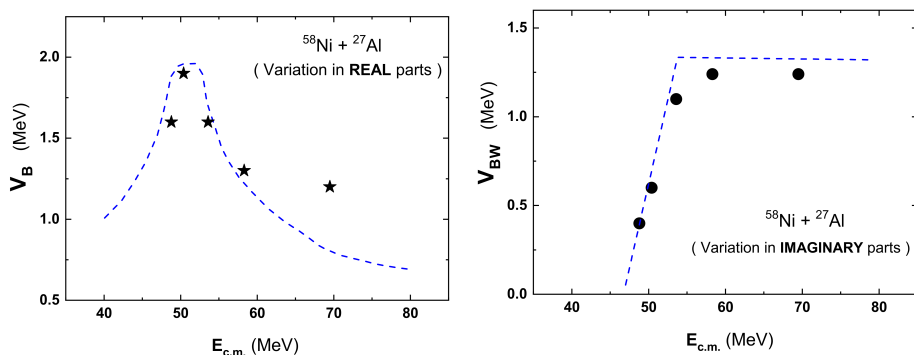


Fig. 5. Variation of optical potential with incident energy. Left: the real part (V_B) varies with incident energy near the Coulomb barrier. The variation is described by a dashed line with dark stars. Right: the imaginary part (V_{BW}) varies with incident energy near the Coulomb barrier. The variation is shown by a dashed line with dark circles.

The imaginary part (V_{BW}) increases when the incident energy increases above the top of the Coulomb barrier and then remains constant at about 1.24 MeV. In the same vicinity, the real part (V_B) increases initially from 1.6 MeV to 1.9 MeV near the Coulomb barrier. Again it decreases rapidly from the top of the barrier until its strength becomes nearly constant (~ 1.25 MeV) at higher energies. The variations surmise the presence of an interesting phenomenon threshold anomaly in the interaction of ^{58}Ni with the ^{27}Al target. The bell-shaped dashed line for the real part and the L-shaped dashed line for the imaginary part shown in the TA graph are obtained from the equation of dispersion relation. Theoretical calculations substantially follow the shapes.

3.3. Study of reflection function $|S_l|$

The variation of the reflection function $|S_l|$ and $|1 - S_l|$ with ' l ' values are depicted in Fig. 6 to observe the dependence on the contributing partial waves at incident energy $E_{\text{cm}} = 69.5$ MeV. As is evident from the plot of $|S_l|$, the partial waves having low ' l ' values are absorbed for which $|S_l|$ almost vanishes. They contribute to nuclear reactions. The partial waves having higher ' l ' values greater than $l = 28$ are effective in the Coulomb region dominated by repulsion. Thus, the plot distinguishes the absorptive domain from the non-absorptive Coulomb domain and shows how the low ' l ' partial waves significantly contribute to the elastic scattering. On the other hand, if the variation of $|1 - S_l|$ is considered, then oscillations in the

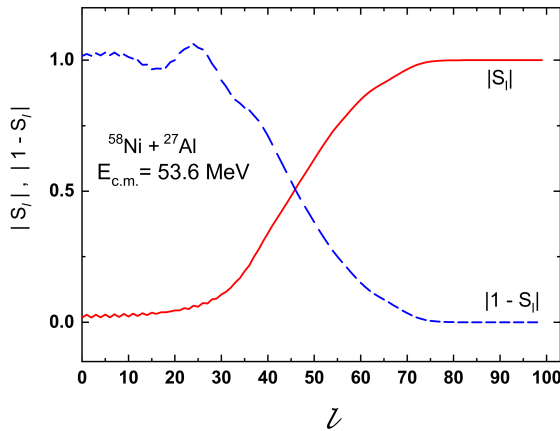


Fig. 6. Plotting of the reflection function $|S_l|$ and $|1 - S_l|$ as functions of ' l ' for the $^{58}\text{Ni} + ^{27}\text{Al}$ system at $E_{\text{cm}} = 69.5$ MeV. Potential parameters are stated above.

elastic cross section at higher energy are expected. When the value of V_{BW} remains small at the surface region, it allows a greater number of partial waves to enter the interior region. Barrier waves are scattered from the barrier. The superposition of internal waves with barrier waves produces correct measured elastic scattering data in presence of a non-trivial feature in the effective potential.

4. Conclusions

We use only three parameters that are energy-dependent for the entire analysis as compared to many parameters of the Woods–Saxon potential. The optical potential used possesses a specific deformation effect at the surface of the nucleus. The deformation controls absorption during nucleus–nucleus scattering. This can be reflected in the analysis of the scattering system. The non-trivial shape of the potential may cause deformation in the Coulomb barrier and particularly such non-trivial deformation helps us explain the elastic scattering data of the system.

Boztosun *et al.* [25] have added two additional real potentials $U_1(r)$ and $U_2(r)$ to the nuclear potential to construct a modified optical potential. The additional terms are derivatives of the Woods–Saxon shape. This technique can modify the shape of optical potential at the surface region. This greatly helps improve the agreement between the experimental values and our theoretical calculations in the elastic scattering. There are many examples of adding extra terms to the nuclear potential which modifies its monotonic variation with the radial distance to account for those effects for fitting the elastic scattering data. In a similar fashion, our optical potential is constructed with a non-trivial formation to accommodate such internal processes in heavy-ion collisions.

We are unable to explain experimental results with the theoretical formalism without considering the non-trivial aspect of our construction. In this regard, we show the results with $R_0 = 0$, and then with $R_0 = R_{0W} = 0$ in Fig. 7 for the system $^{58}\text{Ni}+^{17}\text{Al}$ at $E_{\text{cm}} = 53.6$ MeV to observe the effect of the non-trivial feature. We compare the left plot in the middle row of Fig. 4 with Fig. 7; both the plots are given for the same incident energy, $E_{\text{cm}} = 53.6$ MeV. The theoretical result with $R_0 = 0$ is shown in Fig. 7 with a solid curve, which deviates from the experimental values represented by dark circles. Here, the condition $R_0 = 0$ results in the absence of outer region. Similarly, $R_{0W} = 0$ imposes the condition for the absence of inner region, with which the theoretical result is shown by a horizontal straight segment that largely deviates from the experimental data. Thus, our theoretical calculations agree with the experimental data iff both the regions are taken simultaneously. Hence, by looking at the fittings of calculated elastic scattering values with and without the non-trivial features, we seek its essentiality in our potential.

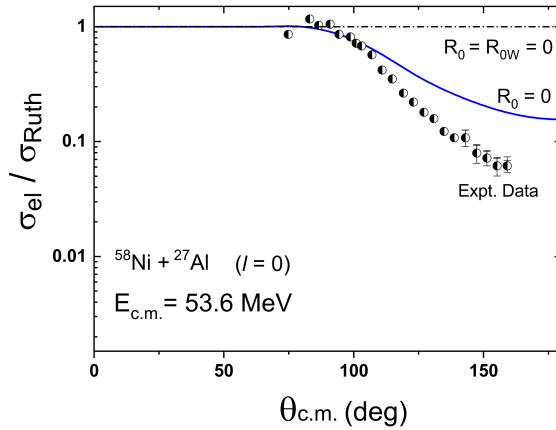


Fig. 7. Comparison of theoretically calculated angular elastic scattering cross sections with experimental values for $^{58}\text{Ni} + ^{27}\text{Al}$ system at $E_{\text{cm}} = 53.6\text{MeV}$ with $R_0 = R_{0w} = 0$, $R_0 = 0$, and the experimental results.

Our theoretical formalism well explains the experimental results for the said system. It works well in the case of the light ^{27}Al -target and heavy ^{58}Ni -projectile. Further, the potential observes the TA phenomenon near the Coulomb barrier of the system considered.

We are thankful to Jajati Kesari Nayak for discussion.

REFERENCES

- [1] M.J. Moravcsik, «The Two-Nucleon Interaction», *Clarendon Press*, Oxford 1963.
- [2] P.E. Hodgson, «The Optical Model of the Nucleon–Nucleus Interaction», *Annu. Rev. Nucl. Sci.* **17**, 1 (1967).
- [3] C. Mahaux, H. Ngô, G.R. Satchler, «Causality and the threshold anomaly of the nucleus–nucleus potential», *Nucl. Phys. A* **449**, 354 (1986).
- [4] A.M. Stefanini *et al.*, «Strong Energy Dependence of the Optical Potential for $^{32}\text{S} + ^{58,64}\text{Ni}$ near the Coulomb Barrier», *Phys. Rev. Lett.* **59**, 2852 (1987).
- [5] D. Pereira *et al.*, «Effect of the threshold anomaly on the fusion cross sections for the systems $^{16}\text{O} + ^{63,65}\text{Cu}$ », *Phys. Lett. B* **220**, 347 (1989).
- [6] I.J. Thompson, M.A. Nagarajan, J.S. Lilley, M.J. Smithson, «The threshold anomaly in $^{16}\text{O} + ^{208}\text{Pb}$ scattering», *Nucl. Phys. A* **505**, 84 (1989).
- [7] M.A. Nagarajan, C.C. Mahaux, G.R. Satchler, «Dispersion Relation and the Low-Energy Behavior of the Heavy-Ion Optical Potential», *Phys. Rev. Lett.* **54**, 1136 (1985).

- [8] D. Abriola *et al.*, «Energy dependence of the optical potential for the $^{16}\text{O} + ^{144}\text{Sm}$ system near the Coulomb barrier», *Phys. Rev. C* **39**, 546 (1989).
- [9] G.R. Sachtler, «Heavy-ion scattering and reactions near the Coulomb barrier and “threshold anomalies”», *Phys. Rep.* **199**, 147 (1991).
- [10] Lin Chengjian *et al.*, «Quasi-elastic Scattering of $^{19}\text{F} + ^{208}\text{Pb}$ System at Near-and Sub-barrier Energies», *Chinese Phys. C* **21**, 872 (1997).
- [11] B.R. Fulton *et al.*, «Energy dependence of the $^{16}\text{O} + ^{60}\text{Ni}$ potential and the optical model dispersion relation», *Phys. Lett. B* **162**, 55 (1985).
- [12] C.J. Lin *et al.*, «Threshold anomaly in the $^{19}\text{F} + ^{208}\text{Pb}$ system», *Phys. Rev. C* **63**, 064606 (2001).
- [13] J. Díaz *et al.*, «The threshold anomaly in the $^{32}\text{S} + ^{40}\text{Ca}$ interaction», *Nucl. Phys. A* **494**, 311 (1989).
- [14] F.W. Byron Jr., R.W. Fuller, «Mathematics of Classical and Quantum Physics», *Inc.*, New York (1992).
- [15] M.E. Brandan *et al.*, «Elastic scattering of $^{58}\text{Ni} + ^{27}\text{Al}$ at near-barrier energies», *Phys. Rev. C* **48**, 1147 (1993).
- [16] B. Bilwes *et al.*, «Folding model analysis of $^{32}\text{S} + ^{32}\text{S}$ elastic scattering at 70, 90, 97.09, 120 and 160 MeV», *Nucl. Phys. A* **473**, 353 (1987).
- [17] J.M. Barrigon *et al.*, «Isotopic effects and surface absorption in $^{35,37}\text{Cl} + ^{24}\text{Mg}$ interactions», *Nucl. Phys. A* **545**, 720 (1992).
- [18] Y. Sugiyama *et al.*, «Transfer cross sections for $^{28}\text{Si} + ^{58,62}\text{Ni}$ », *Phys. Lett. B* **176**, 302 (1986).
- [19] Y. Sugiyama *et al.*, «Contribution of nucleon transfer to the elastic scattering of $^{28}\text{Si} + ^{58,64}\text{Ni}$ near the Coulomb barrier», *Phys. Rev. Lett.* **62**, 1727 (1989).
- [20] K.K. Jena, S.K. Agarwalla, «Analysis of Elastic Scattering of $^{14}\text{N} + ^{90}\text{Zr}$ », in: Y.K. Gupta, R.R. Sahu, S. Santra, A.K. Gupta (Eds.) «Proceedings of the 65th DAE-BRNS Symposium on Nuclear Physics», *Bhabha Atomic Research Centre, DAE Convention Center, Mumbai, India December 1–5, 2021*, p. 329.
- [21] K.K. Jena *et al.*, «Study of Threshold Anomaly in $^{14}\text{N} + ^{56}\text{Fe}$ », in: Y.K. Gupta, R.R. Sahu, S. Santra, A.K. Gupta (Eds.) «Proceedings of the 65th DAE-BRNS Symposium on Nuclear Physics», *Bhabha Atomic Research Centre, DAE Convention Center, Mumbai, India December 1–5, 2021*, p. 437.
- [22] G.S. Mallick, S.K. Agarwalla, B.Sahu, C.S. Shastry, «Analysis of elastic scattering of $^{16}\text{O} + ^{28}\text{Si}$ and $^{12}\text{C} + ^{24}\text{Mg}$ by a new optical potential», *Phys. Rev. C* **73**, 054606 (2006).
- [23] B. Sahu, G.S. Mallick, S.K. Agarwalla, «Soluble complex potential model for heavy-ion collision: resonance and fusion in $^{12}\text{C} + ^{12}\text{C}$ reaction», *Nucl. Phys. A* **727**, 299 (2003).
- [24] J.N. Ginocchio, «A class of exactly solvable potentials. I. One-dimensional Schrödinger equation», *Ann. Phys. (N.Y.)* **152**, 203 (1984).
- [25] I. Boztosun, «New results in the analysis of $^{16}\text{O} + ^{28}\text{Si}$ elastic scattering by modifying the optical potential», *Phys. Rev. C* **66**, 024610 (2002).